4f→5d and anomalous emission in Yb^{2+} doped NaI, SrI_2 and LaI_3 powders prepared by rapid melting and quenching in vacuum

Hendriks, Maurice; van der Kolk, Erik

DOI
10.1016/j.jlumin.2018.11.018

Publication date
2019

Document Version
Final published version

Published in
Journal of Luminescence

Journal of Luminescence 207 (2019) 231–235

Contents lists available at ScienceDirect

Journal of Luminescence

journal homepage: www.elsevier.com/locate/jlumin

4f→5d and anomalous emission in Yb^{2+} doped NaI, SrI_2 and LaI_3 powders prepared by rapid melting and quenching in vacuum

Maurice Hendriks, Erik van der Kolk*

Delft University of Technology, Faculty of Applied Sciences, Luminescent Materials, Mekelweg 15, 2629JB Delft, the Netherlands

A B S T R A C T

The temperature dependent luminescence properties of Yb^{2+} doped in NaI, SrI_2 and LaI_3 powders, prepared by a fast synthesis method involving the rapid melting and quenching in vacuum are reported. The 4f→5d excitation and emission spectra obtained for SrI_2:Yb^{2+} were found to be in accordance with earlier work validating the synthesis methods. In both NaI and SrI_2, doping with Yb^{2+} leads to 5d→4f emission, whereas in LaI_3 no 5d→4f emission was found but instead anomalous emission is observed. In order to understand the observed differences, vacuum referred binding energy (VRBE) schemes were constructed for NaI and LaI_3. For this purpose a NaI:Tm^{3+} sample was prepared, establishing the Tm^{3+} charge transfer energy at 3,5 eV. The VRBE energy scheme of NaI clearly reveals that the 5d states of Yb^{2+} and the other divalent lanthanides are well below the conduction band making 5d→4f emission possible. In LaI_3 the 5d states are almost 1 eV inside the conduction band, which explains the absence of 5d→4f emission and the presence of the anomalous emission.

1. Introduction

Rare earth doped chlorides, bromides and iodides have received a lot of attention as they are considered for application such as laser- and radiation detection crystals and up-conversion phosphors [1,2]. They have also been the subject of many fundamental luminescence studies because of the low phonon energies of these halides enabling the observation of detailed spectroscopic features [3,4]. As halides are strongly hygroscopic, synthesis techniques require special equipment and involved procedures, such as the vertical Bridgman method [5,6]. Although many high quality crystalline, phase pure single crystals and powders have been prepared with great success, a much faster and less involved synthesis could facilitate the study of many more halides with Lanthanide or Transition metal doping and their many possible combinations. In this work we show that synthesis of halides can, in some cases simply be done by melting the starting materials in a vacuum using a flame within minutes. To validate the method we first report on the temperature dependent luminescence properties of Yb^{2+} in SrI_2 powder and show that the luminescence closely resembles that of earlier published work [7]. Then we report on the Yb^{2+} 5d→4f and anomalous emission in NaI and LaI_3 respectively. To explain the results and to predict the luminescent properties of other Lanthanides in these host materials VRBE diagrams were constructed. For this purpose the CT energy of Tm^{3+} in NaI was determined in a sample that was especially prepared for this work.

2. Experimental methods

2.1. Synthesis

The samples were prepared in a glovebox by grinding the starting materials, NaI, SrI_2 and LaI_3 (Alfa Aesar 99.9%) to fine powder and mixing them with 1 mol% of $YbCl_3$ (Sigma Aldrich, 99.99%). For a NaI:Tm^{3+} sample, 1 mol% TmI_2 was used. The mixed powders were placed in silica ampoules, which were closed off with a valve before taking them out of the glove-box. The ampoules were then evacuated by connecting a vacuum pump and opening the valves. The samples were melted as rapidly as possible with a Bunsen burner, without boiling. The burner was removed as soon as all the powder had melted after which the sample was let to cool to room temperature. The recrystallized samples were grinded to a fine powder in a glovebox and loaded in an air tight copper sample holder sealed by a quartz plate and a rubber O-ring for further characterization.

2.2. Characterization

Diffuse reflection measurements were done with a Cathodeon Ltd Deuterium lamp focused into an optical fiber directed at the sample in a hygroscopic sample holder. The diffusely reflected light was collected by an optical fiber connected to a Ocean Optics QE65000 spectrometer. $BaSO_4$ was used as a reference in the same type of hygroscopic sample holder, accounting for the influence of the sample holder as well as the lamp spectrum. Spectra were collected with Ocean Optics SpectraSuite

* Corresponding author.
E-mail address: e.vanderkolk@tudelft.nl (E. van der Kolk).

https://doi.org/10.1016/j.jlumin.2018.11.018
Received 13 March 2018; Received in revised form 5 November 2018; Accepted 8 November 2018
Available online 10 November 2018

software using 500 ms integration time and averaging over 5 scans.

XRD measurements were done with a PANalytical X'pert Pro MPD X-ray diffractometer with a Cu anode operating at 45 kV and 40 mA, producing the following wavelengths: $\lambda_{K\alpha1}$ = 1.540598 Å, $\lambda_{K\alpha2}$ = 1.544426 Å. The diffracted X-rays were detected from 10 to 100 2θ with step-size of 0.0084 and an integration time of 45 s per step.

Excitation and emission spectra were obtained with a photo luminescence excitation and emission setup. The sample, again in a hygroscopic sample holder, was attached to a helium closed cycle refrigerator for low temperature measurements between 10 and 350 K. The sample was illuminated with a OSRAM XBO450W/4Suprasil Xenon light source. The excitation wavelength was selected by a Horiba Gemini 180 monochromator and the emission wavelength with an Princeton Instruments Acton Sp2300 double monochromator. The emission was detected with a Hamamatsu C9100-13 EM-CCD Digital Camera and a Hamamatsu R7600U-03 PMT. All emission and excitation spectra were corrected for the wavelength dependent intensity of the lamp.

3. Results

3.1. SrI_2:1%Yb^{3+}

XRD measurements were carried out to check whether secondary phases had formed. In Fig. 1 the XRD spectra are shown of the untreated starting material together with the doped sample after recrystallization. All the peaks shown in the undoped starting material are in accordance with the database reference. The doped sample does not show any other peaks than those of the undoped sample or the reference, suggesting that the synthesis method has not altered the structure of SrI_2 and that no secondary phases have formed. It can be concluded that the Yb^{2+} and Cl^- ions did not cause any noticeable distortions of the lattice.

The emission and excitation spectra given in Fig. 2 are similar to those found in literature [7].

The two emission bands at 417 and 442 nm are assigned to the spin-allowed (sa) and spin forbidden (sf) $4f^{13}5d \rightarrow 4f^{14}$ transitions from respectively the low spin (LS) and high spin (HS) states of Yb^{2+}. The sf transition intensity increases slightly with temperature whereas the sa decreases. There are multiple processes that can influence the temperature dependence of the sa and sf intensities. One of which is non radiative relaxation to the HS state from which sf emission originates, which is at lower energy than the LS state. This non radiative relaxation is a slow process at low temperatures but becomes faster at higher temperatures as earlier proposed [7,8] and therefore an increase in temperature may induce an increase in sf intensity with respect to the sa intensity.

Self-absorption can amplify the increase of sf transition at higher

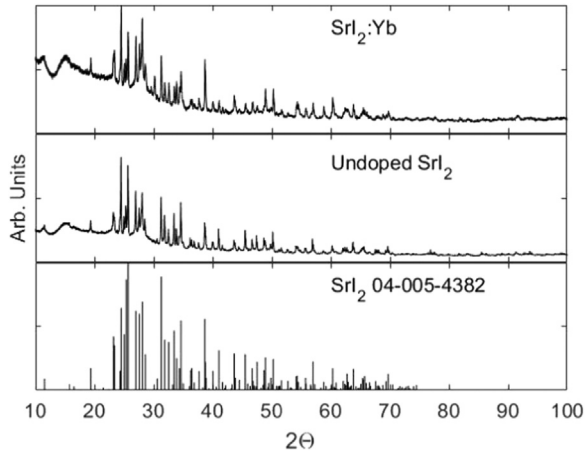

Fig. 1. XRD measurements of undoped SrI_2, SrI_2 doped with Yb and the reference from the ICDD PDF-card 04–005-4382.

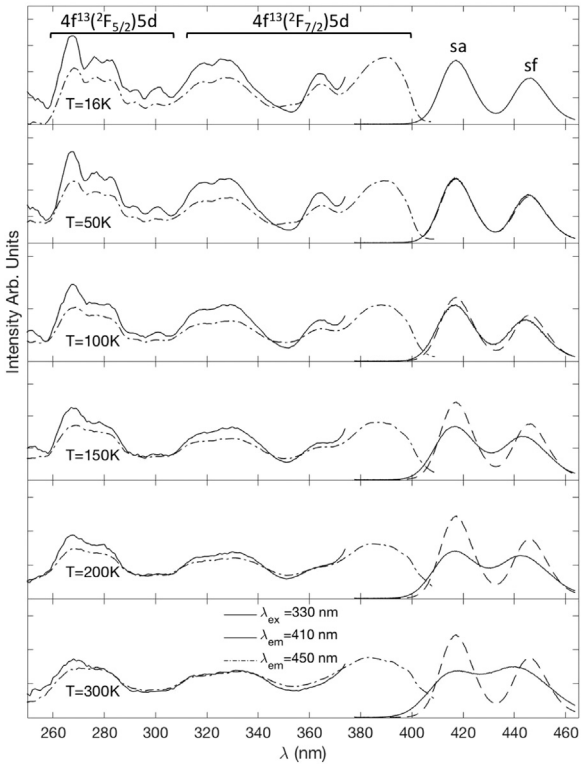

Fig. 2. Emission and excitation spectra of SrI_2:Yb^{2+} between 16 and 300 K. The dashed line in the emission is the emission line at 16 K, repeated in every plot for intensity reference.

temperature. The sa photon can be self-absorbed, after which there is a certain probability of relaxing to the HS state, increasing the sf transition intensity. In addition the broadening of the 5d bands, clearly observable in Fig. 2, increases the overlap between the absorption and emission and thereby the self-absorption efficiency. As self-absorption efficiency depends on the doping ion concentration and is stronger in single crystals compared to powders it is not possible to quantitatively compare the results of [7] with Fig. 2. In the excitation spectra two groups of peaks can be distinguished, the lower energy belonging $4f \rightarrow 4f^{13}[^2F_{7/2}]5d$ transitions and the higher energy to the $4f \rightarrow 4f^{13}[^2F_{5/2}]5d$.

The room temperature diffuse reflection measurement in Fig. 3 is in agreement with the excitation spectrum at T = 300 K of Fig. 2. The three absorption peaks are the same as the three bands observed in the excitation spectrum. No other absorption bands are detected, suggesting that no other non-radiative transitions take place.

3.2. NaI:Yb^{2+}

The XRD spectra of NaI in Fig. 4 show a characteristic Rocksalt structure. All peaks measured in the undoped as well as in the doped sample are in accordance with the lines from the PDF-card. The peaks at higher angles show a duplication as shown in the figure insets. This is due to the difference in wavelength of $\lambda_{K\alpha1}$ and $\lambda_{K\alpha2}$ radiation from the X-ray source. The peaks in the doped sample are somewhat broader, smoothening out the double peak. Na^+ and Yb^{2+} both have an ionic radius of 1.07 A in a coordination number 6 environment [9]. The broadening of the peaks may be explained by the influence of the charge compensating defect that must be present when Yb^{2+} replaces Na^+. The presence of charge compensating defects may cause a slight spread of the lattice spacing, resulting in broader peaks.

The emission and excitation spectra of Yb^{2+} doped NaI shown in Fig. 5 have similarities with that of SrI_2:Yb^{2+}.

PDF-card 01–078-0602.

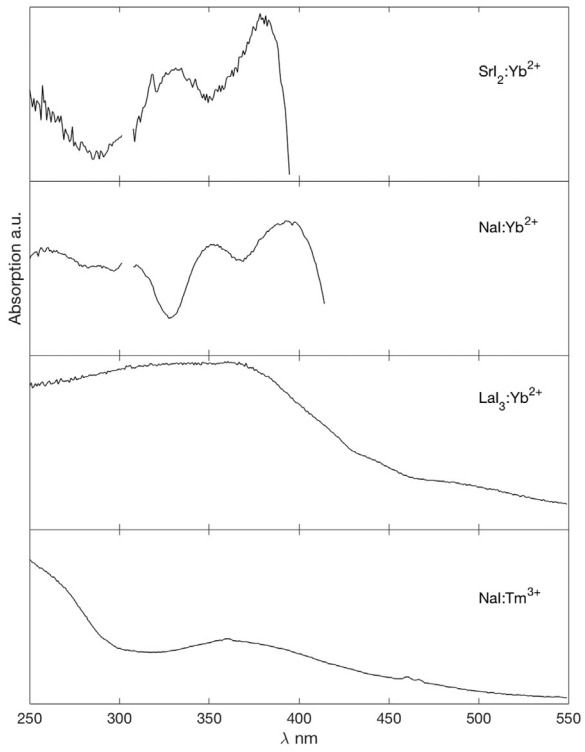

Fig. 3. Absorption spectrum obtained from diffuse reflection measurements at room temperature. The strong emission of $SrI_2:Yb^{2+}$ and $NaI:Yb^{2+}$ caused an unnatural drop towards zero close to the high energy side of the emission.

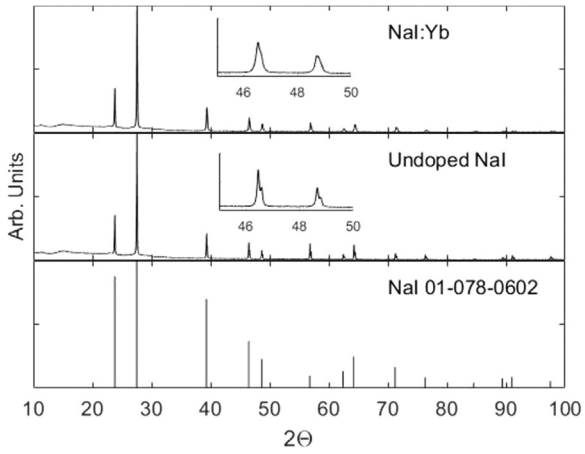

Fig. 4. XRD measurements of untreated NaI, Yb doped NaI, and the reference from ICDD.

The two emission peaks at 427 nm and 464 nm are again the spin allowed and spin forbidden transitions. In this case, however, the sf emission has a higher intensity, even at low temperatures. The sa transition first decreases in intensity with increasing temperature until 300 K to rise again slightly at 350 K. The same processes that play a role in the sa and sf intensities in SrI_2 apply here as well. Thermal population of the LS state can be an explanation for the slight increase in sa and further decrease of sf intensity at 350 K. Regarding the excitation spectra, similar features can be distinguished as in SrI_2. Again the excitation spectrum can be divided into two groups of 5d bands. The lower energy accounts for the $4f \rightarrow 4f^{13}[^2F_{7/2}]5d$ transitions and the higher energy for the $4f \rightarrow 4f^{13}[^2F_{5/2}]5d$. The diffuse reflection of $NaI:Yb^{2+}$ is in accordance with the excitation spectrum. The crystal field splitting ε_{cfs} is expected to be 1.3 eV from the work of Dorenbos [10]. This value for ε_{cfs} is visible as the width of the $4f^{13}[^2F_{5/2}]5d$ bands. The highest energy 5d bands of the $4f^{13}[^2F_{7/2}]5d$ is not clearly visible in the spectrum.

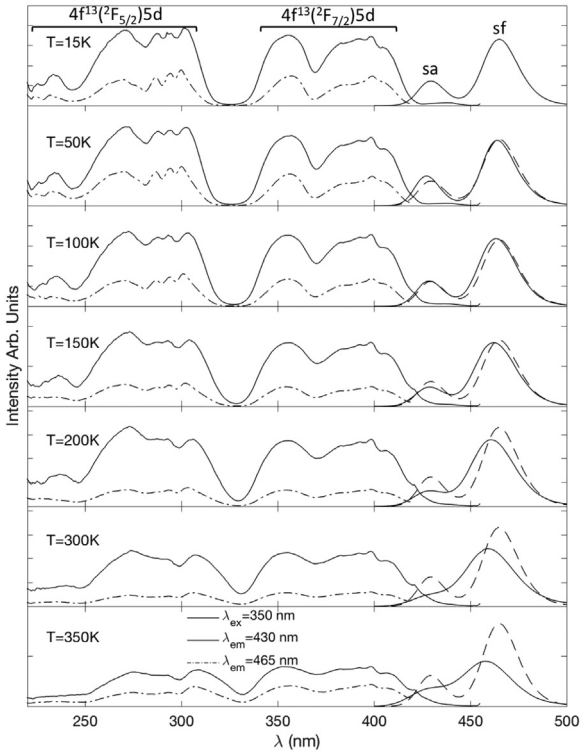

Fig. 5. Emission and excitation spectra of $NaI:Yb^{2+}$ between 15 and 300 K. The dashed line in the emission is the emission line at 15 K, repeated in every plot for intensity reference.

An additional sample of NaI doped with Tm^{3+} was made to determine the Ln^{2+} 4f ground state level for the construction of the VRBE diagram as will be discussed later. In Fig. 3 two absorption bands were detected, one that starts < 290 nm and the other at centered at 360 nm, which are respectively the onset of the band gap and the CT absorption.

3.3. LaI_3

The XRD spectra in Fig. 6 agree with structure of LaI_3. The peaks of the doped and undoped samples match the peaks of the reference from the database. No secondary phases are found.

The emission and excitation spectra show, unlike those of $SrI_2:Yb^{2+}$

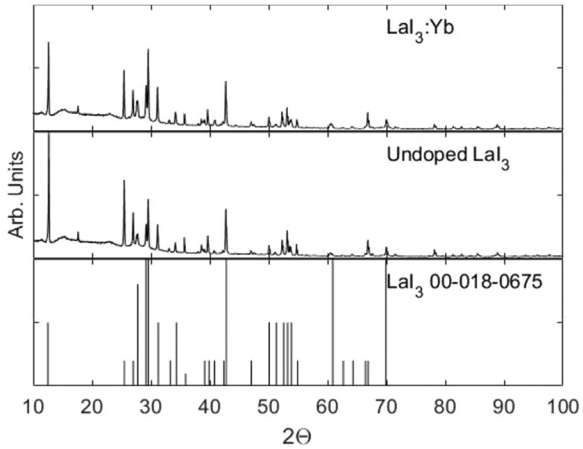

Fig. 6. XRD measurements results of undoped LaI_3, Yb doped LaI_3, and the reference from the ICDD PDF-card 00–018-0675.

and NaI:Yb^{2+}, no 5d→4f emission. The very broad peak around 710 nm is believed to be anomalous emission. The shoulder of this band at 600 nm is an emission of LaI_3 itself. It was also found in [11] where it was ascribed to STE emission. Its temperature dependence found in this work is the same. The excitation spectrum at 300 K consists of 3 bands, around 300, 400 and 500 nm. We assign the part around 500 nm to the 5d states of Yb^{2+} as the energy is in accordance with what can be derived from Eu^{2+} [10]. The 400 nm peak at 300 K shifts to 375 nm at 16 K. The energy of the optical band gap is 3.3 eV (376 nm) at 6 K as reported by [11]. This corresponds to the 400 nm peak at 300 K that shifts to 375 nm at 16 K. The band gap of semiconductors generally decreases for increasing temperatures [12], explaining the shift to around 400 nm at 300 K. The diffuse reflection spectrum in Fig. 3 shows the same shape between 350 and 550 nm.

4. Discussion

The different emission types for Yb^{2+} in NaI and SrI_2 (5d→4f) and LaI_3 (anomalous) can be understood by considering the energy of the lowest 5d state with respect to the conduction band. These relative energies are displayed in so-called VRBE diagrams. The systematic behavior of the Lanthanides allows for the prediction of the spectroscopic properties of the lanthanide of interest when the values for the band gap, the U parameter (which relates the energy of the ground state of a Ln^{2+} with that of Ln^{3+} in the same compound), E^{CT} and the 5d→4f energy is known for any of the other Lanthanides [13]. With these energies a VRBE scheme can be acquired with which the transition energies can be predicted for the lanthanide of interest.

The VRBE schemes presented in this section are compiled with values from literature or measured in this work. The energies used are represented by the arrows in the figures. The relative energies represented by the arrows are placed on the absolute energy scale with the use of the U parameter and the chemical shift model, which places the 4f levels with respect to the vacuum energy [14]. The VRBE of SrI_2 was already published in [15]. The VRBE for NaI is given in Fig. 8.

Arrow 1 is the exciton energy of 5.6 eV from [16]. Arrow 2 (3.0 eV) is the 4f→5d energy of NaI:Eu^{2+} from [17]. E^{CT}, represented by arrow 3 (3.36 eV) is presented in Fig. 3. The 4f→5d energy of NaI:Yb^{2+}, arrow 4 (3 eV), is measured in this work and given in Fig. 5. U is estimated to be 6.25 eV, similar to other iodides like SrI_2, YI_3 and LuI_3. Fig. 9 shows the VRBE diagram for LaI_3.

Arrow 1 is the optical band gap of 3.3 eV from [11]. Arrow 2 represents the 4f→5d transition of Ce^{3+} (2.9 eV) [11]. Arrow 2 can also be used to approximate the Eu^{2+} 4f→5d energy indicated by arrow 3 according to the relation established in [10] between the 4f→5d energy of the di- and trivalent ions. Arrow 4 is the 4f→5d energy of Yb^{2+} measured in this work as the first excitation band in Fig. 7. The U parameter was found in [14]. As no value for E^{CT} is known, the divalent levels are placed with respect to the CB and VB using the U parameter and the energy of the lowest energy 5d level of Ce^{3+} with respect to the CB which is 0.1–0.2 eV [11].

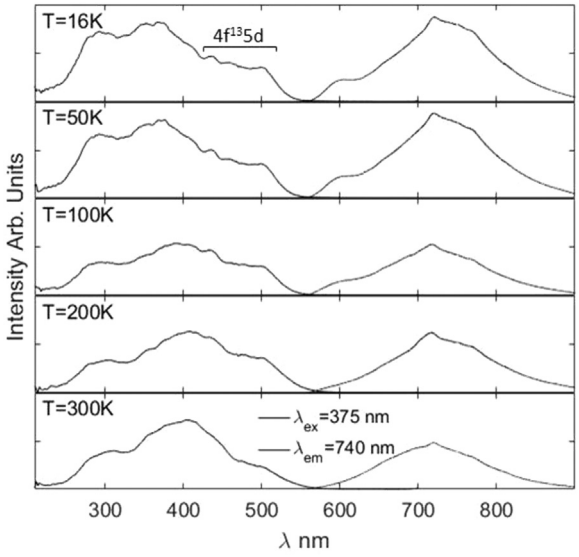

Fig. 7. Emission and excitation spectra of LaI_3:Yb^{2+} between 16 and 300 K.

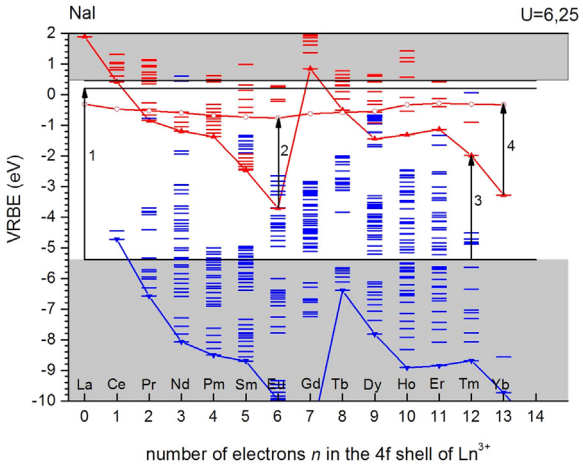

Fig. 8. VRBE scheme of NaI. The arrows indicate the energies used to construct the diagram.

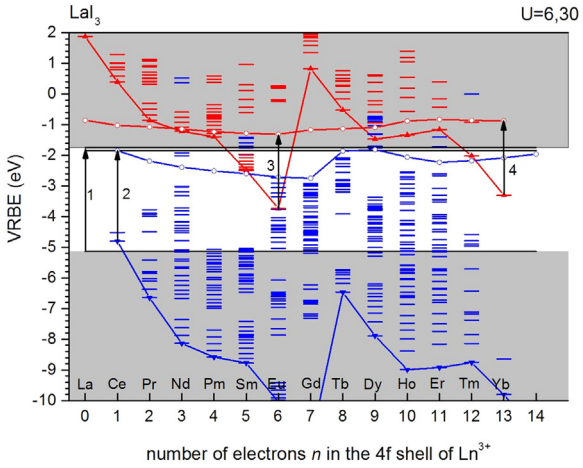

Fig. 9. VRBE scheme of LaI_3.

The VRBE for LaI_3 shows that the first 5d level of Yb^{2+} is inside the CB. From [18] it is known that there will not be any 5d→4f emission when the 5d level is in the conduction band. The electron from the excited 5d level is then delocalized to the surrounding cations, leaving behind an Yb^{3+} impurity. When the system returns to its ground state radiatively, anomalous emission is observed. It is in essence a radiative charge transfer from the cations coordinating Yb^{2+} to the rare earth ion. It is characterized by a very broad peak and a large Stokes' shift. The lowest 4f→5d transition energy, shown in Fig. 9 is 2.43 eV (510 nm). This agrees with the lowest excitation energy in Fig. 7 and the first absorption peak in Fig. 3. It is unclear what the nature of the structure in the anomalous emission band can be. It was reproduced in new, freshly prepared samples and appears to be independent of the detector used.

5. Conclusion

The luminescence of Yb^{2+} in NaI, SrI_2 and LaI_3 prepared by rapid

melting and quenching in vacuum was studied. The results of SrI_2:Yb^{2+} were in agreement with what was found in literature. In NaI:Yb^{2+} 5d→4f emission was observed with spin allowed emission at 427 nm and spin forbidden emission at 464 nm. The E^{CT} of Tm^{3+} in NaI was determined to be 3.5 eV with a diffuse reflection measurement. In LaI_3 no 5d→4f emission was found but anomalous emission was observed instead. By constructing the VRBE diagrams the origin for anomalous emission was found since the lowest 5d bands are located inside the CB. From this, together with the XRD results, we conclude that in these cases the rapid and easy method of synthesis can be used to obtain rare earth doped samples with good enough quality for a first exploration of properties.

Acknowledgments

We thank Prof. P. Dorenbos for helpful discussion about the VRBE diagrams. We thank Ir M. Plokker for his advice on the preparation of the samples. This work is part of the Open technology Program with project number 15024 which is partly financed by the Netherlands Organization for Scientific Research (NWO).

References

[1] K.W. Krämer, P. Dorenbos, H.U. Güdel, C.W.E. van Eijk, Development and characterization of highly efficient new cerium doped rare earth halide scintillator materials, J. Mater. Chem. 16 (27) (2006) 2773–2780, https://doi.org/10.1039/B602762H.

[2] D.R. Gamelin, H.U. Gudel, Upconversion Processes in Transition Metal and Rare Earth Metal Systems, in: H. Yersin (Ed.), Transition Metal and Rare Earth Compounds. Topics in Current Chemistry, 214 Springer, Berlin, Heidelberg, 2001, , https://doi.org/10.1007/3-540-44474-2_1.

[3] J. Grimm, H.U. Güdel, Five different types of spontaneous emission simultaneously observed in Tm2+ doped CsCaBr3, Chem. Phys. Lett. 404 (1–3) (2005) 40–43, https://doi.org/10.1016/j.cplett.2005.01.051.

[4] M. Suta, W. Urland, C. Daul, C. Wickleder, Photoluminescence prop-erties of Yb2+ ions doped in the perovskites CsCaX3 and CsSrX3 (X = Cl, Br, and I) a com-parative study, Phys. Chem. Chem. Phys. 18 (19) (2016) 13196–13208, https://doi.org/10.1039/C6CP00085A 〈http://xlink.rsc.org/?DOI=C6CP00085A〉.

[5] G. Meyer, The synthesis and structures of complex rare-earth halides, Prog. Solid State Chem. 14 (3) (1982) 141–219, https://doi.org/10.1016/ 0079-6786(82)90005-X.

[6] E. Beurer, J. Grimm, P. Gerner, H.U. Güdel, New type of near-infrared to visible photon upconversion in Tm 2+-doped CsCal3, J. Am. Chem. Soc. 128 (10) (2006) 3110–3111, https://doi.org/10.1021/ ja0567790.

[7] M.S. Alekhin, D.A. Biner, K.W. Krämer, P. Dorenbos, Optical and scintillation properties of SrI2:Yb2+, Opt. Mater. 37 (C) (2014) 382–386, https://doi.org/10.1016/j.optmat.2014.06.030.

[8] Z. Pan, C.K. Duan, P.A. Tanner, Electronic spectra and crystal field analysis of Yb2+ in SrCl2, Phys. Rev. B Condens. Matter Mater. Phys. 77 (8) (2008) 1–13, https://doi.org/10.1103/PhysRevB.77.085114.

[9] R.D. Shannon, Revised effective ionic radii and systematic studies of interatomic distances in halides and chalcogenides, Acta Crystallogr.-ica Sect. A 32 (5) (1976) 751–767, https://doi.org/10.1107/S0567739476001551.

[10] P. Dorenbos, Relation between Eu2+ and Ce3+ fd transition energies in inorganic compounds, J. Phys.: Condens. Matter 15 (27) (2003) 4797–4807, https://doi.org/10.1088/0953-8984/15/27/311.

[11] A. Bessiere, P. Dorenbos, C.W.E. Van Eijk, K.W. Krämer, H.U. Güdel, C. De Mello Donega, A. Meijerink, Luminescence and scintillation properties of the small band gap compound LaI3:Ce3+, Nucl. Instrum. Methods Phys. Res., Sect. A: Accel., Spectrometer Detect. Assoc. Equip. 537 (1–2 SPEC. ISS.) (2005) 22–26, https://doi.org/10.1016/j.nima.2004.07.224.

[12] D. Wolpert, P. Ampadu, Managing temperature effects in nanoscale adaptive systems, 2012, 1-174. 〈http://dx.doi.org/10.1007/978-1-4614-0748-5〉.

[13] P. Dorenbos, Modeling the chemical shift of lanthanide 4f electron binding energies, Phys. Rev. B - Condens. Matter Mater. Phys. 85 (16) (2012) 1–10, https://doi.org/10.1103/PhysRevB.85.165107.

[14] P. Dorenbos, Lanthanide 4f-electron binding energies and the nephelauxetic effect in wide band gap compounds, J. Lumin. 136 (2013) 122–129, https://doi.org/10.1016/j.jlumin.2012.11.030.

[15] M.S. Alekhin, R.H. Awater, D.A. Biner, K.W. Krämer, J.T. De Haas, P. Dorenbos, Luminescence and spectroscopic properties of Sm2+ and Er3+ doped SrI2, J. Lumin. 167 (2015) 347–351, https://doi.org/10.1016/j.jlumin.2015.07.002.

[16] Itoh Noria, Defect Processes Induced By Electronic Excitation In Insulators, (1989), https://doi.org/10.1142/0445.

[17] P. Dorenbos, fd transition energies of Divalent Lanthanides in inorganic compounds, J. Phys. Condens. Matter 15 (3) (2003) 575–594, https://doi.org/10.1088/0953-8984/15/3/322.

[18] P. Dorenbos, Anomalous luminescence of Eu2+ and Yb2+ in inorganic compounds, J. Phys.: Condens. Matter 15 (17) (2003) 2645–2665, https://doi.org/10.1088/0953-8984/15/17/318.